Kinetics of the Reactions of Allyl and Propargyl Radicals with CH_3

Vadim D. Knyazev* and Irene R. Slagle*

The Catholic University of America, Department of Chemistry, Washington, D.C. 20064

Received: October 20, 2000; In Final Form: January 16, 2001

The allyl-methyl and propargyl-methyl cross-radical reactions were studied by laser photolysis/photoionization mass spectroscopy. Overall rate constants were obtained in direct real-time experiments in the temperature region 301−800 K and bath gas (helium) density (3−36) × 10^{16} atom cm^{-3}. The observed overall C_3H_5 + CH_3 (1) and C_3H_3 + CH_3 (2) rate constants demonstrate negative temperature dependencies. Master equation modeling of collisional effects indicates that the C_3H_5 + CH_3 reaction is near its high-pressure limit under all experimental conditions used. Minor corrections for the falloff effects (on average, 18% at the highest temperature) applied to the experimental values result in the high-pressure-limit temperature dependence of the rate constant of reaction 1: $k_1^\infty = 1.55 \times 10^{-9}\ T^{-0.54}\exp(117\ K/T)$ cm^3 $molecule^{-1}$ s^{-1}. The temperature dependence of k_1^∞ combined with the thermochemistry of reaction 1 results in the rate constants of the reverse reaction of thermal decomposition of 1-C_4H_8 $k_{-1}^\infty(T) = 1.1 \times 10^{16}\exp(-39100\ K/T)$ s^{-1}. On the other hand the C_3H_3 + CH_3 reaction is not near the high-pressure limit and falloff in reaction 2 cannot be neglected at temperatures above 500 K. Falloff corrections applied to reaction 2, on average, reach a factor of 2 at 800 K and introduce substantial uncertainties in the extrapolated high-pressure-limit rate constant values. The evaluated high-pressure-limit rate constants of reaction 2 can be represented with the expression $k_2^\infty = 6.80 \times 10^{-11}\exp(130K/T)$ cm^3 $molecule^{-1}$ s^{-1}. C_4H_8 and C_4H_6 were identified as primary products of the reactions 1 and 2, respectively.

I. Introduction

Radical−radical cross-combination reactions constitute an integral part of the overall mechanisms of oxidation and pyrolysis of hydrocarbons.[1,2] Reliable rate and branching data on this type of reaction are sparse as these reactions are difficult to study experimentally due to the high reactivity of the chemical species involved. Stabilized alkenyl and alkynyl radicals play important roles in the combustion of hydrocarbons. The stability and low reactivity of stabilized alkenyl radicals has been linked to the antiknock effects of fuel additives such as ethyl *tert*-butyl ether (ETBE).[3,4] Propargyl radicals have been implicated as important intermediates in the mechanisms of formation of soot in hydrocarbon flames (see, for example, refs 5−8). Because of electron delocalization, allyl and propargyl radicals, the simplest members of these classes of radicals, are relatively stable and unreactive with respect to thermal decomposition and reaction with molecular oxygen. This stability results in the accumulation of these radicals in flames. Thus, other removal processes, including radical−radical reactions, become important and accurate knowledge of the rate constants of the reactions of allyl and propargyl radicals with other reactive intermediates, such as radicals and atoms, is needed in order to model the behavior of these species in flames.

In this work, we present the results of a direct experimental investigation of the reactions of allyl and propargyl radicals with methyl radical.

$$C_3H_5 + CH_3 \rightarrow \text{products} \quad (1)$$

$$C_3H_3 + CH_3 \rightarrow \text{products} \quad (2)$$

Reactions 1 and 2 were studied by means of laser photolysis/photoionization mass spectrometry. Overall rate constants were obtained in the temperature region 301−800 K and at bath gas (helium) densities in the range (3−36) × 10^{16} atom cm^{-3}.

Reactions 1 and 2 have been studied experimentally only at room temperature. Garland and Bayes[9] used the laser photolysis/photoionization mass spectrometry technique to obtain the rate constant of reaction 1 at 300 K and 4 Torr of argon bath gas, $k_1 = (6.5 \pm 2.0) \times 10^{-11}$ cm^3 $molecule^{-1}$ s^{-1}. Fahr and Nayak[10] studied reaction 2 at room temperature and 50 Torr using laser photolysis of precursors, final product analysis, and kinetic modeling. These authors determined the value of $k_2 = (1.5 \pm 0.3) \times 10^{-10}$ cm^3 $molecule^{-1}$ s^{-1}.

This article is organized as follows. Section I is an introduction. Section II presents the experimental method and the results. Falloff modeling is described in section III and discussion is given in section IV.

II. Experimental Section

In this section, first, the experimental apparatus used is described. Second, photolysis routes of free radical precursors are characterized. The method of determination of rate constants and the associated kinetic mechanism is explained next, followed by a detailed description of experimental procedure used. Finally, the experimental results are presented.

Apparatus. Details of the experimental apparatus[11] and method[12] have been described previously. Only a brief description is presented here. Pulsed 193 nm unfocused collimated radiation from a Lambda Physik 201 MSC ArF excimer laser was directed along the axis of a 50 cm long 1.05 cm i.d. heatable tubular quartz reactor coated with boron oxide or poly(dimethylsiloxane).[13] The laser was operated at 4 Hz and at a fluence of 120−170 mJ/pulse. The energy flux of the laser radiation inside the reactor was in the range of 6−17 mJ/cm^2 per pulse depending on the degree of laser beam attenuation.

10.1021/jp003890d CCC: $20.00
Published on Web 02/28/2001

Gas flowing through the tube at ≈4 m s^{-1} (in order to replace the photolyzed gas with a fresh reactant gas mixture between the laser pulses) contained free radical precursors in low concentrations and the bath gas, helium. The gas was continuously sampled through a 0.04 cm diameter tapered hole in the wall of the reactor (gas-sampling orifice) and formed into a beam by a conical skimmer before it entered the vacuum chamber containing the photoionization mass spectrometer (PIMS). As the gas beam traversed the ion source, a portion was photoionized using an atomic resonance lamp, mass selected in an EXTREL quadrupole mass filter, and detected by a Daly detector.[14] Temporal ion signal profiles were recorded from 10 to 30 ms before each laser pulse to 15−35 ms following the pulse by using an EG&G ORTEC multichannel scaler interfaced with a PC computer. Typically, data from 1000 to 15000 repetitions of the experiment were accumulated before the data were analyzed. The sources of ionizing radiation were chlorine (8.9−9.1 eV, CaF_2 window, used to detect C_3H_5 and C_3H_3), hydrogen (10.2 eV, MgF_2 window, used to detect CH_3, C_4H_8, C_4H_6, C_3H_2, C_3H_4, C_3H_5Br, C_6H_{10}, and C_3H_3Br), and argon (11.6−11.9 eV, LiF window, used to detect C_3H_2) resonance lamps.

Photolysis of Radical Precursors. Radicals were produced by 193 nm photolysis of corresponding precursors. The photolysis of acetone at 193 nm, which was used in this study as the source of methyl radicals, was shown by Lightfoot et al.[15] to proceed predominantly (>95%) via channel 3a under conditions similar to those used in the current work.

$$CH_3C(O)CH_3 \xrightarrow{193\ nm} 2CH_3 + CO \quad (3a)$$

$$\rightarrow H + CH_2C(O)CH_3 \quad (3b)$$

$$\rightarrow CH_4 + CH_2CO \quad (3c)$$

Photolysis channels 3b and c are known[15] to occur to a minor degree, <3% and < 2%, respectively. The initial concentration of CH_3 radicals produced by the photolysis can thus be determined by measuring the photolytic depletion of $CH_3C(O)CH_3$ (the fraction of acetone decomposed due to photolysis) using time-resolved photoionization mass spectrometry (see below).

Allyl radicals were produced by the photolysis of allyl bromide[16] or 1,5-hexadiene.[17]

$$C_3H_5Br \xrightarrow{193\ nm} C_3H_5 + Br \quad (4a)$$

$$\rightarrow C_3H_4 + HBr \quad (4b)$$

$$C_6H_{10} \xrightarrow{193\ nm} 2\ C_3H_5 \quad (5a)$$

$$\rightarrow \text{other products} \quad (5b)$$

Propargyl radicals were produced by the photolysis of propargyl bromide[18] or 1,3-butadiene.[18]

$$C_3H_3Br \xrightarrow{193\ nm} C_3H_3 + Br \quad (6a)$$

$$\rightarrow C_3H_2 + HBr \quad (6b)$$

$$C_4H_6 \xrightarrow{193\ nm} C_3H_3 + CH_3 \quad (7a)$$

$$\rightarrow \text{other products} \quad (7b)$$

Radical precursors were obtained from Aldrich (acetone (>99.9%), allyl bromide (99.0%), 1,5-hexadiene (97.0%), and 1,3-butadiene (>99%)) and TCI (propargyl bromide (>97%)) and were purified by vacuum distillation prior to use. Helium (>99.999%, <1.5 ppm of O_2, MG Industries) was used without further purification.

Method of Determination of Rate Constants. CH_3 and R radicals (R = C_3H_5 or C_3H_3) were produced simultaneously by the 193 nm photolysis of a mixture of corresponding precursors highly diluted in the helium carrier gas (>99.9%). The rate constant measurements were performed using a technique analogous to that applied by Niiranen and Gutman to the studies of the $SiH_3 + CH_3$ and $Si(CH_3)_3 + CH_3$ kinetics,[19] which is a further development of the method used by Garland and Bayes to study a series of radical cross-combination reactions.[9] Experimental conditions (in particular, the two precursor concentrations) were selected to create a large excess of initial concentrations of methyl radicals over the total combined concentration of all the remaining radicals formed in the system. The initial concentration of methyl radicals was always 22−180 times higher than that of R. The concentration of R radicals was always less than 2×10^{11} molecules cm^{-3}. Under these conditions, the self-recombination of methyl radicals was essentially unperturbed by the presence of the other radicals. At the same time, the kinetics of R decay was completely determined by the reaction with CH_3 and unaffected either by self-reaction or by reactions with other active species formed in the system, such as the side products of precursor photolysis.

Heterogeneous loss was the only additional sink of methyl and R radicals that had to be taken into account. Thus, the kinetic mechanism of the important loss processes of CH_3 and R in these experiments is as follows:

$$R + CH_3 \rightarrow \text{products} \quad (1 \text{ or } 2)$$

$$CH_3 + CH_3 \rightarrow C_2H_6 \quad (8)$$

$$R \rightarrow \text{heterogeneous loss} \quad (9 \text{ or } 10)$$

$$CH_3 \rightarrow \text{heterogeneous loss} \quad (11)$$

(Here, reaction 9 is the wall loss of C_3H_5 and reaction 10 is that of C_3H_3). For this mechanism and for the initial conditions described above, the system of first order differential equations can be solved analytically.

$$\frac{[CH_3]_t}{[CH_3]_0} = \frac{k_{11}\exp(-k_{11}t)}{2k_8[CH_3]_0(1-\exp(-k_{11}t)) + k_{11}} \quad (I)$$

$$\frac{[R]_t}{[R]_0} = \exp(-k_9 t)\left[\frac{k_{11}}{2k_8[CH_3]_0(1-\exp(-k_{11}t)) + k_{11}}\right]^{k_1[CH_3]_0/2k_8[CH_3]_0} \quad (II)$$

Equations I and II are written for the case R = C_3H_5 (k_1 and k_9 rate constants are used for the R + CH_3 and wall loss reactions, respectively). For the R = C_3H_3 case, k_1 and k_9 need to be replaced with k_2 and k_{10}.

Experimental signal profiles of CH_3 and R radicals (see subsection Procedure below) were fitted with eqs I and II, respectively, to obtain the values of the $k_8[CH_3]_0$ and $k_1[CH_3]_0$ (or $k_2[CH_3]_0$) products. The k_1 and k_2 rate constants were then obtained by dividing the experimental $k_1[CH_3]_0$ and $k_2[CH_3]_0$

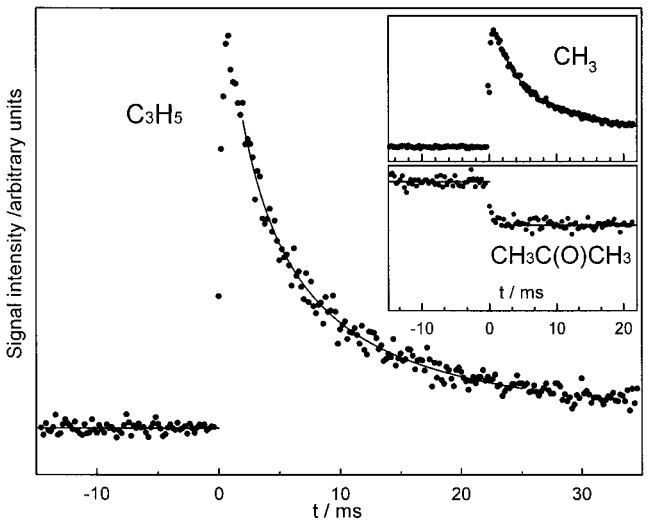

Figure 1. Examples of temporal ion signal profiles obtained in the experiments to measure k_1. $T = 305$ K, [He] $= 1.20 \times 10^{17}$ atoms cm^{-3}, [C_3H_5Br] $= 1.25 \times 10^{11}$ molecules cm^{-3}, [$CH_3C(O)CH_3$] $= 1.59 \times 10^{13}$ molecules cm^{-3}, [C_3H_5]$_0 \leq 4.3 \times 10^{10}$ molecules cm^{-3}, [CH_3]$_0 = 3.24 \times 10^{12}$ molecules cm^{-3}. Lines are the results of fits with formulas I (for CH_3) and II (for C_3H_5).

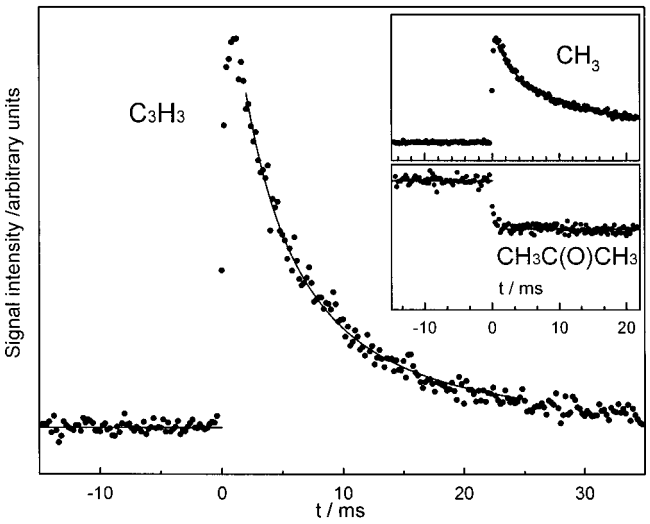

Figure 2. Examples of temporal ion signal profiles obtained in the experiments to measure k_2. $T = 600$ K, [He] $= 1.20 \times 10^{17}$ atoms cm^{-3}, [C_4H_6] $= 3.11 \times 10^{11}$ molecules cm^{-3}, [$CH_3C(O)CH_3$] $= 1.70 \times 10^{13}$ molecules cm^{-3}, [C_3H_3]$_0 \leq 1.46 \times 10^{11}$ molecules cm^{-3}, [CH_3]$_0 = 4.85 \times 10^{12}$ molecules cm^{-3}. Lines are the results of fits with formulas I (for CH_3) and II (for C_3H_3).

values by [CH_3]$_0$ determined by measuring the photolytic depletion of acetone (see below). An important feature of this method is that exact knowledge of the initial concentration of R is not required for the determination of the rate constants. In this respect, the approach is similar to the pseudo-first-order method frequently applied to studies of kinetics of second-order reactions.

Procedure. In experiments with only one of the radical precursors present in the reactor under conditions where radical−radical reactions are negligible (low precursor concentration or/and low laser intensity), the radical kinetics (CH_3, C_3H_5, or C_3H_3) was that of purely exponential decay. The rate of the decay did not depend on the concentration of the precursor or the laser intensity but was affected by the wall conditions of the reactor (such as coating and history of exposure to reactive mixtures). This decay was attributed to heterogeneous loss processes. The rate constants of heterogeneous loss of methyl (k_{11}) and allyl (k_9) or propargyl (k_{10}) radicals were determined in separate sets of measurements. The wall loss rates of the C_3H_5 and C_3H_3 radicals were in the ranges 3−10 and 3−29 s^{-1}, respectively, and were minor compared to the rates of radical decay due to the reactions under study (reactions 1 and 2). The wall loss rate constant of CH_3 decay was usually in the range 0−11 s^{-1}.

In the experiments to measure the R + CH_3 reaction rate constants, the initial (high) concentration of methyl radicals was determined by measuring the photolytic depletion of acetone (the fraction of acetone decomposed due to photolysis). The value of the decomposition ratio (the relative decrease in the precursor concentration upon photolysis) was obtained directly from the acetone ion signal profile (Typical profiles are shown in Figures 1 and 2.) and corrected for the ion signal background. The background (less than 10% of the acetone signal) was mainly due to a low constant concentration of acetone molecules in the mass-spectrometer vacuum chamber and the interaction of the scattered UV light from the resonance lamp with the high voltage target of the Daly detector. The method of correction for the ion signal background is described in detail in ref 12. Initial concentrations of R (R = C_3H_5 or C_3H_3) were evaluated by monitoring the photolytic depletion of corresponding precursors. Since products other than C_3H_5 or C_3H_3 were also produced in the photolysis (reactions 4−7), only upper limit values to the concentration of R could be obtained.

The procedure of determination of the R + CH_3 rate constants for each set of experimental conditions consisted of the following sequence of measurements:

1. Kinetics of heterogeneous loss of R (determination of k_9 (or k_{10})). Only the R radical precursor is present in the reactor (along with the helium carrier gas which is always present).

2. Decomposition ratio of the R radical precursor (determination of an upper limit of [R]$_0$).

3. Kinetics of heterogeneous loss of CH_3 (determination of k_{11}). Only acetone is in the reactor. The photolyzing laser beam is significantly attenuated to provide low CH_3 concentrations.

4. Decomposition ratio of acetone (determination of [CH_3]$_0$). Both radical precursors are in the reactor, from here to step 6. Low or no attenuation of the laser bean is used (high CH_3 concentrations), from here to step 6.

5. Kinetics of methyl radical decay (determination of the k_8[CH_3]$_0$ product).

6. Kinetics of R radical decay in the presence of methyl radicals (determination of the k_1[CH_3]$_0$ product and k_1 (or the k_2[CH_3]$_0$ product and k_2)).

Measurements 4 and 5 were repeated in reverse order after monitoring the kinetics of R radicals in the presence of methyl radicals in order to ensure the stability of initial concentrations of CH_3. Also, the stability of the heterogeneous loss rate constants during the set of measurements was checked experimentally.

Typical temporal profiles of [$CH_3C(O)CH_3$] (photolytic precursor of CH_3 radicals), [CH_3], and [R] (R = C_3H_5 or C_3H_3) are shown in Figures 1 and 2. The lines through the experimental [CH_3] and [R] vs time profiles are obtained from fits of these dependencies with expressions I and II, respectively. In each experiment (consisting of the set of measurements described above), the value of the k_8[CH_3]$_0$ product was obtained from the fit of the [CH_3] vs time dependence (measured in step 5) using the value of k_{11} (wall loss of CH_3) determined in step 3. Then the value of the k_1[CH_3]$_0$ product (or k_2[CH_3]$_0$) was obtained from the fit of the [R] vs time dependence using the k_9 (or k_{10}), k_{11}, and k_8[CH_3]$_0$ values obtained in steps 1, 3,

TABLE 1: Conditions and Results of Experiments to Determine k_1

T/K	[He][a]	[prec.][b]	$[C_3H_6O]^b$	$[C_3H_5]_0{}^b$	$[CH_3]_0{}^b$	I^c	k_9/s^{-1}	k_{11}/s^{-1}	$k_8{}^d$	$k_1{}^d$	$k/k^{\infty e}$	$k_1{}^{\infty\,d,f}$	F^f
301	12.0	5.99[g]	358.6	0.66	28.7	8	3.2	4.3	4.26 ± 1.13	10.43 ± 2.08	1.00	10.43	1.20
305	12.0	3.13[h]	164.5	1.08	34.4	17	10.1	0.0	4.73 ± 1.13	9.60 ± 1.22	1.00	9.60	1.13
305	12.0	1.25[h]	159.3	0.43	32.4	17	10.1	0.0	4.39 ± 0.97	9.40 ± 1.49	1.00	9.40	1.16
305	12.0	1.25[h]	518.7	0.43	111.0	16	10.1	0.0	3.65 ± 1.40	10.47 ± 3.91	1.00	10.47	1.37
306	12.0	6.31	291.8	1.21	62.9	16	3.2	3.3	3.99 ± 1.02	10.66 ± 1.65	1.00	10.66	1.16
306	12.0	1.94	70.1	0.37	14.5	16	3.2	3.3	4.62 ± 1.46	10.83 ± 2.67	1.00	10.83	1.25
400	12.0	1.97	169.1	0.34	46.2	16	5.2	4.1	3.31 ± 0.98	7.89 ± 1.87	1.00	7.89	1.24
400	12.0	1.97	67.8	0.34	18.0	16	5.2	4.1	3.68 ± 0.94	8.42 ± 1.54	1.00	8.42	1.18
600	12.0	1.91[h]	185.6	0.70	68.0	16	8.3	7.3	1.80 ± 0.44	5.88 ± 1.15	0.99	5.95	1.24
600	12.0	1.91[h]	180.4	0.36	34.3	6	8.3	7.3	1.77 ± 0.50	5.55 ± 1.08	0.99	5.61	1.24
800	12.0	5.47	162.9	1.52	64.9	18	5.5	12.6	0.95 ± 0.24	4.49 ± 0.59	0.92	4.88	1.35
800	12.0	5.47	155.9	0.45	18.23	4	5.5	12.6	0.88 ± 0.31	4.41 ± 0.69	0.92	4.79	1.38
800	3.0	2.41	191.0	0.59	73.2	16	9.3	9.8	0.70 ± 0.15	4.12 ± 0.61	0.82	5.01	1.57
800	36.0	2.51	160.6	0.61	55.5	16	5.3	11.3	1.27 ± 0.35	4.34 ± 0.66	0.96	4.50	1.27

[a] Concentration of the bath gas (helium) in units of 10^{16} atom cm^{-3}. [b] Concentrations of the allyl radical photolytic precursor, acetone, C_3H_5, and CH_3 in units of 10^{11} molecules cm^{-3}. Concentration of C_3H_5 is an upper limit (see text). [c] Laser intensity in mJ $pulse^{-1}$ cm^{-2}. [d] In units of 10^{-11} cm^3 $molecule^{-1}$ s^{-1}. [e] Calculated falloff correction factor (section III). [f] $k_1{}^\infty$ are obtained by dividing the experimental k_1 values by the calculated k/k^∞ factors. F is the uncertainty factor of $k_1{}^\infty$ (i.e., upper and lower limiting values of $k_1{}^\infty$ can be obtained by multiplying or dividing the optimum value by F). [g] Poly(dimethylsiloxane) reactor wall coating was used. Boron oxide coated reactor was used in all other experiments. [h] C_3H_5Br (allyl bromide) was used as a photolytic precursor of C_3H_3. C_6H_{10} (1,5-hexadiene) was used in all other experiments.

TABLE 2: Conditions and Results of Experiments to Determine k_2

T/K	[He] [a]	[prec.][b]	$[C_3H_6O]^b$	$[C_3H_3]_0{}^b$	$[CH_3]_0{}^b$	I^c	$k_{10}/\ s^{-1}$	$k_{11}/\ s^{-1}$	$k_8{}^d$	$k_2{}^d$	$k/k^{\infty e}$	$k_2{}^{\infty\,d,f}$	F^f
301	12.0	5.91[g,h]	358.4	0.54	28.7	8	2.9	4.3	4.20 ± 1.15	10.71 ± 2.68	0.98	10.87	1.37
304	12.0	1.35	196.4	0.53	35.8	15	20.8	1.0	4.34 ± 1.59	11.82 ± 3.66	0.98	12.00	1.37
304	12.0	1.35	205.1	0.26	18.4	7	20.8	1.0	4.19 ± 1.24	9.01 ± 2.86	0.98	9.15	1.29
304	12.0	1.35	69.1	0.53	11.8	15	20.8	1.0	4.44 ± 1.69	9.99 ± 2.33	0.98	10.14	1.38
305	12.0	7.93[h]	231.3	1.23	3.46	14	29.0	0.0	4.52 ± 1.67	10.44 ± 3.40	0.98	10.60	1.30
400	12.0	0.99	259.6	0.31	56.0	16	14.7	2.4	3.42 ± 1.21	9.92 ± 2.61	0.94	10.59	1.55
400	3.0	5.41[h]	195.8	0.90	41.6	14	19.0	5.1	2.52 ± 0.64	8.08 ± 1.61	0.85	9.52	1.44
400	36.0	5.41[h]	186.2	0.90	33.8	14	12.0	0.0	3.90 ± 1.23	8.32 ± 2.01	0.97	8.56	1.33
600	12.0	3.11	170.1	1.46	48.5	15	10.9	4.3	1.53 ± 0.43	5.48 ± 0.96	0.70	7.84	1.80
600	12.0	3.11	171.6	0.76	25.6	7	10.9	4.3	1.55 ± 0.49	5.17 ± 0.94	0.70	7.39	1.81
600	12.0	3.11	412.9	1.46	114.4	15	10.9	4.3	1.58 ± 0.49	5.33 ± 1.23	0.70	7.62	1.88
600	12.0	8.34[h]	422.0	1.96	116.1	15	14.1	4.3	1.54 ± 0.59	5.82 ± 1.60	0.70	8.33	1.95
800	3.0	1.89	184.1	0.53	53.9	15	14.0	34.0	0.30 ± 0.14	2.82 ± 0.52	0.24	11.64	2.98[i]
800	36.0	1.55	182.6	0.44	42.5	12	6.4	2.9	1.23 ± 0.33	3.94 ± 0.94	0.55	7.18	2.24[i]
800	36.0	1.55	177.3	0.22	21.2	6	12.3	2.9	1.56 ± 0.47	4.27 ± 0.86	0.55	7.78	2.17[i]

[a] Concentration of the bath gas (helium) in units of 10^{16} atom cm^{-3}. [b] Concentrations of the propargyl radical photolytic precursor, acetone, C_3H_3, and CH_3 in units of 10^{11} molecules cm^{-3}. Concentration of C_3H_3 is an upper limit (see text). [c] Laser intensity in mJ $pulse^{-1}$ cm^{-2}. [d] In units of 10^{-11} cm^3 $molecule^{-1}$ s^{-1}. [e] Calculated falloff correction factor (section III). [f] $k_2{}^\infty$ are obtained by dividing the experimental k_2 values by the calculated k/k^∞ factors. F is the uncertainty factor of $k_2{}^\infty$ (i.e., upper and lower limiting values of $k_2{}^\infty$ can be obtained by multiplying or dividing the optimum value by F). [g] Poly(dimethylsiloxane) reactor wall coating was used. Boron oxide coated reactor was used in all other experiments. [h] C_3H_3Br (propargyl bromide) was used as a photolytic precursor of C_3H_3. C_4H_6 (1,3-butadiene) was used in all other experiments. [i] Uncertainties of $k_2{}^\infty$ estimated for the data at 800 K are, most likely, unrealistically large. See section IV for a discussion of the uncertainty range of $k_2{}^\infty$(T) dependence.

and 5, respectively. Finally, the value of k_1 (or k_2) was obtained by dividing the $k_1[CH_3]_0$ product by $[CH_3]_0$ determined in step 4.

The sources of error in the measured experimental parameters such as temperature, pressure, flow rate, signal count, etc., were subdivided into statistical and systematic and propagated to the final values of the rate constants using different mathematical procedures for propagating systematic and statistical uncertainties.[20] In particular, the effects of uncertainties in the heterogeneous radical decay rates and in the $k_8[CH_3]_0$ product on the derived k_1 and k_2 values were evaluated for all experiments. The error limits of the experimentally obtained rate constant values reported in this work represent a sum of 2σ statistical uncertainty and estimated systematic uncertainty.

Experimental Results

The rate constants of reactions 1 and 2 were determined at temperatures between 301 and 800 K and bath gas densities [He] = (3−36) × 10^{16} atom cm^{-3}. Conditions and results of all experiments are listed in Tables 1 and 2. It was verified experimentally that these rate constants did not depend on the photolyzing laser intensity, initial concentrations of R and CH_3, reactor wall coating, or the nature of the photolytic precursor of R. The rate constants of reactions 1 and 2 did not demonstrate any pressure dependence within the experimental uncertainties.

Although the measurement of k_8 (CH_3 recombination) was not the goal of the current work, the experiments provided rate constant values for the $CH_3 + CH_3$ reaction. Uncertainty in the k_8 values (Tables 1 and 2) is rather high, up to 40% of the values, due to the fact that the experimental conditions were optimized for most accurate determination of k_1 and k_2, not k_8. The results obtained are in good agreement with those previously measured.[12,21]

Arrhenius plots of the $C_3H_5 + CH_3$ and $C_3H_3 + CH_3$ rate constants (k_1 and k_2) are shown in Figures 3 and 4. The observed rate constants decrease with increasing temperature. These temperature dependencies can be represented with parametric

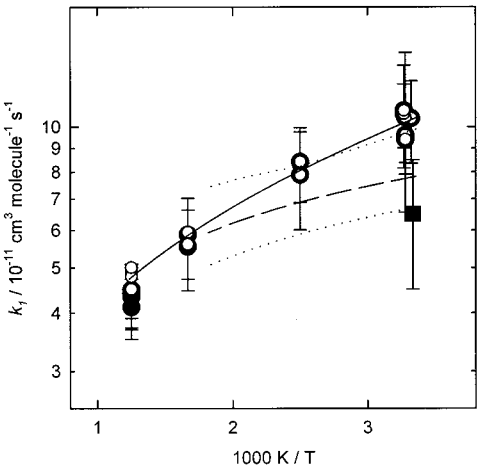

Figure 3. Temperature dependencies of the experimentally obtained values of k_1 (filled circles) and extrapolated values of k_1^∞ (open smaller circles). Square represents the k_1 value reported by Garland and Bayes.[9] Solid line is the modified Arrhenius fit of the k_1^∞(T) dependence given by formula XIII. Dashed and dotted lines are the central and the limiting values of k_1^∞ calculated using the "geometric mean rule" (see text).

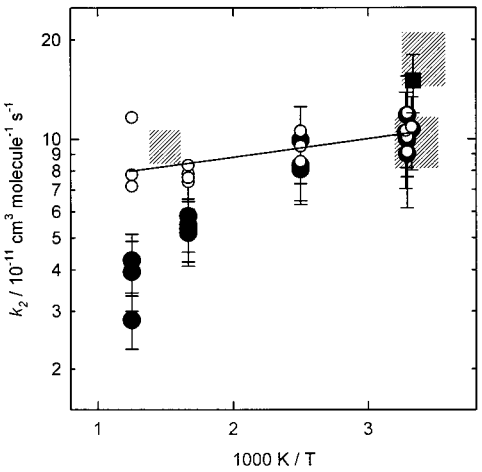

Figure 4. Temperature dependencies of the experimentally obtained values of k_2 (filled circles) and extrapolated values of k_2^∞ (open smaller circles). Square represents the k_2 value reported by Fahr and Nayak.[10] Solid line is the Arrhenius fit of the k_1^∞(T) dependence given by formula XIV. Shaded areas demonstrate the uncertainty ranges of k_1^∞ calculated using the "geometric mean rule" and the values of k_{14} reported by Morter et al.[22] (upper shaded area at room temperature), Atkinson and Hudgens[23] and Fahr and Nayak[10] (lower shaded area at room temperature), and Alkemade and Homann[24] (shaded area between 623 and 723 K) (see text).

fits given by the following expressions:

$$k_1 = 6.46 \times 10^{-8} T^{-1.08} \exp(-90K/T) \text{ cm}^3 \text{ molecule}^{-1} \text{ s}^{-1} \quad \text{(III)}$$

$$k_2 = 2.91 \times 10^{-4} T^{-2.27} \exp(-561K/T) \text{ cm}^3 \text{ molecule}^{-1} \text{ s}^{-1} \quad \text{(IV)}$$

These expressions have 15% and 20% uncertainties, respectively. Experimental error limits of individual data points are given in Tables 1 and 2.

C_4H_8 and C_4H_6 were detected as products of reactions 1 and 2, respectively, with product rise times matching those of the C_3H_5 and C_3H_3 decays. Attempts were made to detect the C_3H_4 and C_3H_2 products of the possible disproportionation channels of the $C_3H_5 + CH_3$ and $C_3H_3 + CH_3$ reactions. C_3H_4 was produced by the photolysis of both precursors used for the production of C_3H_5 (C_3H_5Br and C_6H_{10}). The shapes of the C_3H_4 signal temporal profiles were those of "step" function both in the presence and absence of CH_3 in the reactor. No slowly rising part of the signal could be detected indicating that the disproportionation channel of reaction 1 can be of only minor (if any) importance. No signal of C_3H_2 could be detected in the experiments on reaction 2.

III. Falloff Correction.

Experimental data on the $C_3H_5 + CH_3 \rightarrow C_4H_8$ (1) and $C_3H_3 + CH_3 \rightarrow C_4H_6$ (2) reactions were obtained at low bath gas pressures, where falloff can be of importance. This section describes the assessment of pressure effects (falloff from the high-pressure limit) for reactions 1 and 2. First, the method of obtaining approximate values of the microscopic energy-dependent rate constants for C_4H_8 and C_4H_6 decomposition based on the inverse Laplace transform of the temperature dependence of the high-pressure-limit recombination rate ($k^\infty(T)$) is presented. Second, the iterative procedure of master equation modeling performed with the purpose of evaluating the falloff corrections (k/k^∞) is described. Finally, the high-pressure-limit rate constants of reactions 1 and 2 are obtained by applying the falloff corrections to the experimental values and associated uncertainties are described.

Microscopic Rates via Inverse Laplace Transform of the High-Pressure-Limit Recombination Rate. The temperature dependence of a high-pressure-limit rate constant of a dissociation reaction ($k_d^\infty(T)$) can be presented as a Laplace transform of the product of the microscopic energy dependent rate constant $k_d(E)$ and the density-of-states function of the active molecule (see, for example, ref 25). Thus, information on the $k_d^\infty(T)$ or the related (via equilibrium constant) rate of the reverse recombination reaction, $k_r^\infty(T)$, can be used to obtain the $k_d(E)$ function. The derivation presented here is based on the earlier works by Forst,[26] Pritchard,[27] and Davis et al.[28]

The high-pressure-limit rate constant of a dissociation reaction

$$AB \rightarrow A + B \quad (12)$$

can be presented in the form[25,29,30]

$$k_d^\infty(\beta) = \frac{1}{Q_{AB}^a(\beta)} \int_o^\infty k_d(E) \rho_{AB}(E) \exp(-\beta E) dE \quad \text{(V)}$$

Here, $\beta = (k_B T)^{-1}$ is the reduced inverse temperature, k_B is the Boltzmann constant, and $\rho_{AB}(E)$ and $Q_{AB}^a(\beta)$ are the density-of-states and partition functions of the active[25,29,30] degrees of freedom of the AB molecule, respectively. It is assumed here that all rotational effects due to angular momentum conservation are averaged over the thermal distribution and incorporated into an effective $k_d(E)$ function. The equilibrium constant of reaction 12 can be given by

$$K_{eq}(\beta) \equiv \frac{k_r^\infty}{k_d^\infty} = \frac{Q_{AB}^i(\beta) Q_{AB}^a(\beta)}{Q_A(\beta) Q_B(\beta)} \left(\frac{h^2 \beta}{2\pi\mu}\right)^{3/2} \exp(-\beta E_0) \quad \text{(VI)}$$

Here, $Q_{AB}^i(\beta)$ is the partition functions of the inactive, or adiabatic,[25,29,30] degrees of freedom of AB, $Q_A(\beta)$ and $Q_B(\beta)$ are partition functions of A and B, h is the Planck constant, μ is the reduced mass, and E_0 is the 0 K reaction enthalpy. All partition functions include only internal degrees of freedom (electronic, vibrational, and rotational). The term in parentheses appears from the contribution of the translational degrees of freedom.

From eqs V and VI one obtains

$$k_r^\infty = \frac{Q^i_{AB}(\beta)}{Q_A(\beta)Q_B(\beta)}\left(\frac{h^2\beta}{2\pi\mu}\right)^{3/2}\int_o^\infty k_d(E)\rho_{AB}(E)\exp(-\beta(E-E_0))dE \quad \text{(VII)}$$

Let us present the temperature dependence of the high-pressure-limit recombination rate constant in the modified Arrhenius form

$$k_r^\infty = A_r^\infty \beta^n \exp(-\beta E_r^\infty) \quad \text{(VIII)}$$

and assume that the two-dimensional rotation of AB as a whole is inactive while the remaining one-dimensional AB rotation together with all internal rotations and vibrations forms the pool of the active degrees of freedom.[25,29,30] Then $Q^i_{AB}(\beta)$ can be presented as

$$Q^i_{AB}(\beta) = (B^i_{AB}\beta)^{-1} \quad \text{(IX)}$$

where B^i_{AB} is the rotational constant of the inactive two-dimensional rotation (with symmetry factor incorporated) and, combining eqs VII, VIII, and IX, one obtains

$$\int_o^\infty k_d(E)\rho_{AB}(E)\exp(-\beta E)dE = A_r^\infty B^i_{AB}\left(\frac{2\pi\mu}{h^2}\right)^{3/2} Q_A(\beta)Q_B(\beta)\beta^{n-1/2}\exp(-\beta(E_0+E_r^\infty)) \quad \text{(X)}$$

The left side of this equation is a Laplace transform of the $k_d(E)\rho_{AB}(E)$ function, and therefore, $k_d(E)\rho_{AB}(E)$ can be obtained by performing the inverse Laplace transform of the right side of eq X numerically. An interesting case occurs when $n = {}^1/_2$. The term with $\beta^{n-1/2}$ disappears and eq X can be presented as

$$L[k_d(E)\rho_{AB}(E)] = A_r^\infty B^i_{AB}\left(\frac{2\pi\mu}{h^2}\right)^{3/2} L[\rho_P(E-E_0-E_r^\infty)] \quad \text{(XI)}$$

Here, $\rho_P(E)$ is the density-of-states function of a "pseudo-molecule" with internal degrees of freedom formed from the combined internal degrees of freedom of molecules A and B ($Q_P(\beta) \equiv Q_A(\beta)Q_B(\beta) = L[\rho_P(E)]$).

Thus, $k_d(E)$ function can be obtained from

$$k_d(E) = A_r^\infty B^{\infty i}_{AB}\left(\frac{2\pi\mu}{h^2}\right)^{3/2}\frac{\rho_P(E-E_0-E_r^\infty)}{\rho_{AB}(E)} \quad \text{(XII)}$$

Expression XII can be easily evaluated by computing the densities of states using existing methods for harmonic oscillators, free and hindered rotors.[31−33]

Master Equation Modeling and Falloff Corrections. Falloff factors (k/k^∞) were calculated for each experimental data point using the solution of the master equation. The formulation of master equation for recombination reactions and its relation to that of reverse decomposition reactions can be found elsewhere.[29,34] The *ChemRate* program[35] was used in all calculations, including the calculations of the densities of states required to evaluate the $k(E)$ dependencies via expression XII. The method of Gaynor et al.[36] was used to solve the steady-state master equation. The exponential-down[29,37] model of collisional energy transfer was used.

The properties of the model were selected in an iterative process. First, the experimentally obtained $k_r(T)$ temperature dependencies (Figures 3 and 4) were assumed to represent those of the high-pressure-limit and were fitted with expression VIII using fixed $n = {}^1/_2$. The obtained A_r^∞ and E_r^∞ parameters were used to evaluate the $k(E)$ functions. These $k(E)$ dependencies were used in master equation modeling which, in turn, yielded the calculated k/k^∞ falloff factors. Then the experimental $k_r(T)$ values were divided by these k/k^∞ falloff factors to obtain the "corrected" high-pressure-limit rate constants. The procedure was then repeated until convergence. Convergence was achieved for reaction 1 after two iterations (within less than 1%) and for reaction 2 after three iterations (within less than 4%). Molecular properties such as vibrational frequencies and rotational constants used in the calculations are listed in Table 3.

TABLE 3: Properties of Molecules Used in Models of Reactions 1 and 2

Enthalpies of Formation (kJ mol^{-1})				
$\Delta_f H^0_{298}(C_3H_5) = 184.5 \pm 2.1$[38]			$\Delta_f H^0_{298}(C_3H_3) = 339.0 \pm 4.0$[39]	
$\Delta_f H^0_{298}(CH_3) = 146.0 \pm 1.0$ [48,49]			$\Delta_f H^0_{298}(1\text{-}C_4H_8) = 0.1 \pm 1.0$[40]	
$\Delta_f H^0_{298}(1\text{-}C_4H_6) = 165.2 \pm 0.9$[41]				
Vibrational Frequencies (cm^{-1})				
C_3H_5:[42]	426, 514, 544, 738, 801, 912, 983, 1071, 1182, 1247, 1390, 1464, 1487, 3019, 3021, 3054, 3107, 3107			
C_3H_3:[43]	3462, 3172, 2028, 1475, 1068, 644, 476, 386, 3268, 987, 621, 351			
CH_3:[44]	3184 (2), 3002, 1383(2), 580			
1-C_4H_8:[45]	283, 331, 387, 417, 652, 759, 813, 900, 912, 956, 976, 1054, 1160, 1206, 1259, 1313, 1394, 1407, 1455, 1467, 1474, 1507, 2842, 2859, 2883, 2915, 2920, 2964, 2974, 3050			
1-C_4H_6:[50−52]	3332, 2988, 2925, 2920, 2116, 1470, 1446, 1385, 1322, 1070, 1008, 840, 634, 509, 2988, 2939, 1462, 1261, 1090, 782, 630, 344, 213			
Rotational Constants (cm^{-1}), Symmetry Numbers (σ, No. of Minima in Parentheses If Different), and Rotational Barriers (kJ mol^{-1})				
C_3H_5:[46]	$B = 0.5658$	$\sigma = 2$		
C_3H_3:[47]	$B = 0.9787$	$\sigma = 2$		
CH_3:[44]	$B = 7.6036$	$\sigma = 6$		
1-C_4H_8:[53,54]	$B = 0.7522$	$\sigma = 1$		(one-dimensional active)
	$B = 0.1369$	$\sigma = 1$		(two-dimensional inactive)
	$B = 5.849$	$\sigma = 3$	$V_o = 1104$	(CH_3 torsion, active)
	$B = 2.194$	$\sigma = 1(3)$	$V_o = 666$	(C_2H_5 torsion, active, 3 minima)
1-C_4H_6:[50−52]	$B = 0.9056$	$\sigma = 1$		(1-dimensional active)
	$B = 0.14379$	$\sigma = 1$		(2-dimensional inactive)
	$B = 5.301$	$\sigma = 3$	$V_o = 1060$	(CH_3 torsion, active)

The choice of collisional energy transfer parameter, $\langle\Delta E\rangle_{down}$ (average energy transferred per deactivating collision with the bath gas)[29,37] can be important in such modeling if the reaction under study is far from the high-pressure-limit conditions. The values of $\langle\Delta E\rangle_{down}$ for C_4H_8 and C_4H_6 used here were based on analogy with the results of Knyazev and Tsang obtained for a molecule of similar size, *sec*-C_4H_9.[55] These authors modeled the chemically and thermally activated decomposition of *sec*-C_4H_9 to reproduce the experimental literature data obtained over a wide range of temperatures (195−680 K). The modeling yielded $\langle\Delta E\rangle_{down}$ proportional to temperature: $\langle\Delta E\rangle_{down}$(*sec*-$C_4H_9$) = 0.52 × ($T$/K) cm^{-1}. A similar proportional dependence was obtained earlier for the decomposition of ethyl radical.[56,57] Collisional energy transfer parameters are known to increase with vibrational energy. References 58−66 can be consulted for reviews of the current literature. On the basis of the results presented in these studies, one can expect a proportional

dependence of $\langle\Delta E\rangle_{all}$ (the average energy transferred per collision) on energy for a hydrocarbon molecule of C_4H_x size. This will mean an approximately square-root dependence for $\langle\Delta E\rangle_{down}$ ($\langle\Delta E\rangle_{down} \sim E^{1/2}$). The above $\langle\Delta E\rangle_{down}$(*sec*-$C_4H_9$) vs T dependence was obtained at the energy barrier height for the *sec*-C_4H_9 decomposition, 31 kcal mol^{-1}, while the reactions of decomposition of C_4H_8 and C_4H_6 have barriers of 77.5 and 74.6 kcal mol^{-1}. Scaling in accordance with the $\langle\Delta E\rangle_{down} \sim E^{1/2}$ dependence yields an approximate expression $\langle\Delta E\rangle_{down} = 0.8 \times (T/\mathrm{K})$ cm^{-1} for C_4H_8 and C_4H_6 decomposition which was used in master equation modeling.

The $\langle\Delta E\rangle_{down}$ values estimated by the above, rather crude, method have large uncertainties. Therefore, to assess the effects of these uncertainties on the results of falloff modeling, calculations were also performed with the proportionality coefficient in the $\langle\Delta E\rangle_{down}$ vs T dependence changed by a factor of 2 in both directions.

The values of the k/k^{∞} falloff correction coefficients obtained in the modeling are listed in Tables 1 and 2. Relative uncertainties of extrapolation to the high-pressure limit were estimated as twice the differences (on a logarithmic scale) between the k/k^{∞} values obtained using the $\langle\Delta E\rangle_{down} = 0.8 \times (T/\mathrm{K})$ cm^{-1} and the $\langle\Delta E\rangle_{down} = 0.4 \times (T/\mathrm{K})$ cm^{-1} formulas for the $\langle\Delta E\rangle_{down}$ temperature dependence. The final uncertainty values of the high-pressure-limit rate constants listed in Tables 1 and 2 (presented as uncertainty factors) were obtained by adding the extrapolation uncertainties to the experimental ones.

As can be expected, the largest falloff corrections (smallest k/k^{∞} values) were obtained at the highest experimental temperature, 800 K. It was found that, while reaction 1 is very close to the high-pressure limit, reaction 2 is noticeably further in the falloff region under the conditions of the experiments. For reaction 1, the lowest $k/k^{\infty} = 0.82$ was calculated. $k/k^{\infty} = 0.24$ was obtained for reaction 2 under the same conditions (800 K and [He] $= 3 \times 10^{16}$ atom cm^{-3}). Thus, the uncertainty of extrapolation is significantly less for reaction 1 (maximum of 37%) than for reaction 2 (maximum factor of 2.5).

The high-pressure-limit rate constants of reactions 1 and 2 obtained by the above extrapolation of experimental results are displayed in Figures 3 and 4 (smaller open circles). Their temperature dependencies can be represented by the following expressions:

$$k_1^{\infty} = 1.55 \times 10^{-9} T^{-0.54} \exp(117K/T)\ \mathrm{cm^3\ molecule^{-1}\ s^{-1}} \quad \text{(XIII)}$$

$$k_2^{\infty} = 6.80 \times 10^{-11} \exp(130K/T)\ \mathrm{cm^3\ molecule^{-1}\ s^{-1}} \quad \text{(XIV)}$$

The estimated uncertainty of expression XIII is 15% at temperatures 300−600 K and increases to 36% at 800 K. That of expression XIV increases with temperature from 24% at room temperature to 36% at 400 K, a factor of 1.8 at 600 K, and a factor of 3 at 800 K. The uncertainty estimated at 800 K using the above procedure is, probably, too large: the upper limiting value combined with the data obtained at lower temperatures would result in an unrealistic positive temperature dependence. A more realistic uncertainty range for k_2^{∞} is proposed in the next section.

IV. Discussion

This work presents the first direct determination of the rate constants of reactions $C_3H_5 + CH_3$ (1) and $C_3H_3 + CH_3$ (2) as functions of temperature. Two earlier studies[9,10] reported room-temperature values of k_1 and k_2. Garland and Bayes[9] studied reaction 1 among several other cross-radical reactions using a laser photolysis/photoionization mass spectrometry method similar to the one employed in the current investigation. These authors, however, used literature values of the rate constants of the $CH_3 + CH_3$ and $C_3H_5 + C_3H_5$ reactions to evaluate initial radical concentrations. Knowledge of both C_3H_5 and CH_3 concentrations was needed in these experiments. Thus, the resultant k_1 value ($(6.5 \pm 2.0) \times 10^{-11}$ cm^3 molecule^{-1} s^{-1}) was dependent on the accuracy of the radical recombination rate constants used by the authors. Fahr and Nayak[10] studied reaction 2 at room temperature and 50 Torr using laser photolysis of precursors, GC/MS product analysis, and kinetic modeling. Their value of $k_2 = (1.5 \pm 0.3) \times 10^{-10}$ cm^3 molecule^{-1} s^{-1} was derived from modeling of the experimentally obtained final products distributions. These authors identified the major products of reaction 2 as approximately 60% of 1-butyne and 40% of 1,2-butadiene. The values of k_1 and k_2 reported in refs 9 and 10 are plotted in Figures 3 and 4 together with the results of the current work. As can be seen from the plots, although the results of the current and earlier studies of reactions 1 and 2 do not coincide exactly, the reported uncertainty limits overlap for both reactions.

The high-pressure-limit rate constants of the reaction between allyl and methyl radicals (1) obtained by a minor extrapolation of the experimental results (section III) display a pronounced negative temperature dependence (eq XIII), as can be expected for a barrierless radical−radical reaction. The temperature dependence of k_2^{∞}, the high-pressure-limit rate constant of the $C_3H_3 + CH_3$ reaction, is more uncertain. This uncertainty is due to the larger extrapolation to the high-pressure limit required in the case of reaction 2 than in the case of reaction 1. The difference between reactions 1 and 2 in terms of the relative positions of the experimental pressure range relative to the falloff scale is, primarily, due to the differences in the densities of states of 1-C_4H_8 (product of reaction 1) and 1-butyne (product of reaction 2). The density of states of 1-C_4H_8 is larger than that of 1-C_4H_6 since 1-butene has two internal rotational degrees of freedom while 1-butyne has only one. In the falloff calculations, 1-butyne was assumed to be the only product of reaction 2. Although the experimental results of Fahr and Nayak indicate the importance of the second channel, that of formation of 1,2-butadiene, the existence of this second channel will not have any drastic influence on the falloff calculations since the density of states of 1,2-butadiene can be expected to be similar to that of 1-butyne (only one internal rotation is present in both of these molecules).

The method of estimating the uncertainty of extrapolation to the high-pressure limit (twice the difference between the k/k^{∞} values obtained using the $\langle\Delta E\rangle_{down} = 0.8\times(T/\mathrm{K})$ cm^{-1} and the $\langle\Delta E\rangle_{down} = 0.4\times(T/\mathrm{K})$ cm^{-1} dependencies, see section III) yields uncertainty values at 800 K, the highest experimental temperature of this work, that are probably too large. The upper limiting values of k_2^{∞} thus obtained for 800 K would result in an unrealistic positive temperature dependence of k_2^{∞}. Therefore, an uncertainty range limited, on the lower end, by the lower limit to the experimentally obtained (in the falloff) rate constant values and, on the upper end, by the upper limit to the room-temperature k_2^{∞} value can be proposed. Thus, the following "central" values and uncertainty range are recommended:

best evaluation:

$$k_2^{\infty} = 6.80 \times 10^{-11} \exp(130\mathrm{K}/T)\ \mathrm{molecule^{-1}\ cm^3\ s^{-1}} \quad \text{(XIV)}$$

lower limit: $k_2^{\infty} \geq 2.33 \times 10^{-4} T^{-2.27} \exp(-561\text{K}/T)$ molecule^{-1} cm^3 s^{-1} (XVII)

upper limit: $k_2^{\infty} \leq 1.27 \times 10^{-10}$ molecule^{-1} cm^3 s^{-1} (XVIII)

Garland and Bayes[9] used their experimental data on radical cross reactions to test the validity of the "geometric mean rule"[9,67,68]

$$k_{AB} = 2(k_{AA}k_{BB})^{1/2} \quad \text{(XV)}$$

frequently used to estimate rate constants of cross radical reactions (k_{AB}) of the type A + B from the values of k_{AA} and k_{BB}, the rate constants of the A + A and B + B self-reactions. Such comparison is also performed in the current work. The rate constants of methyl radical self-reaction

$$CH_3 + CH_3 \rightarrow C_2H_6 \quad (8)$$

are well-known. Two recent "global fits"[69,70] of falloff data provide parametrization for the rate constants that differ very little (less than 5%) in the high-pressure limit. Most of the experimental data used in these parametrizations come from the experimental study of Slagle et al.[21] who used the experimental technique and the apparatus employed in the current work. These authors reported a ± 20% uncertainty in their experimental rate constant values. Thus, in the calculations according to the "geometric mean rule," we used the parametrization of Hessler and Ogren[70] ($k_8^{\infty} = 8.78 \times 10^{-11} \exp(-T/723\text{ K})$ cm^3 molecule^{-1} s^{-1}) with 20% uncertainty.

The rate constants of the allyl radical self-reaction

$$C_3H_5 + C_3H_5 \rightarrow \text{products} \quad (13)$$

have been reported by several groups.[17,71,72] Tulloch et al. reported $k_{13} = (2.65 \pm 0.2) \times 10^{-11}$ cm^3 molecule^{-1} s^{-1} at 295 K and the

$$k_{13}(T) = 1.69 \times 10^{-11} \exp(132\text{ K}/T)\text{ cm}^3\text{ molecule}^{-1}\text{ s}^{-1} \quad (T = 293-571\text{ K}) \quad \text{(XVI)}$$

temperature dependence. Jenkin et al.[72] reported the room-temperature value of $k_{13} = (3.0 \pm 0.5) \times 10^{-11}$ cm^3 molecule^{-1} s^{-1}. Finally, Boyd et al.[71] obtained $k_{13} = (2.6 \pm 0.2) \times 10^{-11}$ cm^3 molecule^{-1} s^{-1} within the temperature range 400−540 K. In all of these studies, allyl radicals were detected spectroscopically and the reported k_{13} values were linearly dependent on the absorption cross section of C_3H_5, which had to be determined independently. In the calculations, we use the temperature dependence of Tulloch et al.[17] (eq XVI) with the uncertainty of ± 0.2 × 10^{-11} cm^3 molecule^{-1} s^{-1}. However, the upper and the lower limiting values used were those of all three studies combined. For example, at room temperature the upper limit of k_{13} was taken as 3.5×10^{-11} cm^3 molecule^{-1} s^{-1} (from the upper limit of Jenkin et al.) and the lower limit as 2.4×10^{-11} cm^3 molecule^{-1} s^{-1} (from the lower limit of Tulloch et al.).

The resultant k_1 values calculated using eq XV (the "geometric mean rule") using the "central" values of k_8 and k_{13} are shown in Figure 3 by the dashed line. The upper and lower limiting values (calculated using the upper and lower limits of k_8 and k_{13}) are shown by the dotted lines. As can be seen from the plot, the uncertainties of the experimental and the calculated rate constants overlap. The combined experimental uncertainties of k_1, k_8, and k_{13} do not allow a more certain assessment of the validity of the "geometric mean rule" as applied to reaction 1.

A similar uncertainty is observed for reaction 2. Four experimental studies of the self-reaction of propargyl radicals

$$C_3H_3 + C_3H_3 \rightarrow \text{products} \quad (14)$$

are available in the literature. At room temperature, the value of the rate constant reported by Morter et al.,[22] $k_{14} = (1.2 \pm 0.2) \times 10^{-10}$ cm^3 molecule^{-1} s^{-1}, is a factor of 3 larger than the values obtained by Atkinson and Hudgens[23] and Fahr and Nayak,[10] $(4.3 \pm 0.6) \times 10^{-11}$ cm^3 molecule^{-1} s^{-1} and $(4.0 \pm 0.4) \times 10^{-11}$ cm^3 molecule^{-1} s^{-1}, respectively. Alkemade and Homann[24] reported $k_{14} = 6.54 \times 10^{-11}$ cm^3 molecule^{-1} s^{-1} (no uncertainties were reported) between the temperatures of 623 and 723 K. k_2 values and uncertainty ranges were calculated using the "geometric mean rule," eq XV, by the same method as for reaction 1 (see above). Figure 4 illustrates the results. At room temperature, the uncertainty ranges of the calculated rate constants obtained with the k_{14} values of Morter et al., Atkinson and Hudgens, and Fahr and Nayak are represented by two shaded areas on the plot. At higher temperatures (623−723 K), a shaded area represents the upper and lower limits calculated using k_{14} reported by Alkemade and Homann (This uncertainty range is likely to be even wider due to unknown error limits of the k_{14} value of Alkemade and Homann). Approximate agreement within the combined uncertainty ranges is achieved between the experimental k_2 values obtained in the current work (extrapolated to the high-pressure limit at higher temperatures) and the values calculated using k_{14} of Atkinson and Hudgens,[23] Fahr and Nayak,[10] and Alkemade and Homann.[24] The k_2 values calculated using $k_{14} = (1.2 \pm 0.2) \times 10^{-10}$ cm^3 molecule^{-1} s^{-1} reported by Morter et al.[22] are noticeably higher than the experimental ones. No certain conclusion about the adequacy of the "geometric mean rule" can be drawn, however, until the controversy regarding the k_{14} values is resolved.

The values of k_1^{∞} obtained in the current work, combined with the known thermochemistry of reaction 1, can be used to evaluate the high-pressure-limit rate constants of the reverse reaction of 1-C_4H_8 decomposition. The k_{-1}^{∞} values thus obtained can be represented with the expression

$$k_{-1}^{\infty}(T) = 1.1 \times 10^{16} \exp(-39100\text{ K}/T)\text{ s}^{-1} \quad \text{(XIX)}$$

evaluated for the experimental temperature range of this work, 301−800 K. The uncertainty of this expression changes from a factor of 6 at room temperature to the factors of 4 at 400 K, 2.7 at 600 K, and 2.5 at 800 K. This uncertainty originates primarily in the error limits of the heats of formation of 1-C_4H_8,[40] C_3H_5,[38] and CH_3[48,49] (overall uncertainty in the reaction 1 enthalpy is 4.1 kJ mol^{-1}). Rate constants of reaction −2, the reverse of the $C_3H_3 + CH_3$ recombination reaction 2, cannot be evaluated using the same approach because of the unknown distribution of products in reaction 2. Although Fahr and Nayak reported an approximate ratio of 1-butyne to 1,2-butadiene at room temperature as 1.5 (60% and 40%, respectively), the temperature dependence of this value is unknown.

Acknowledgment. This research was supported by Division of Chemical Sciences, Office of Basic Energy Sciences, Office of Energy Research, U.S. Department of Energy under Grant DE-FG02-94ER1446.

References and Notes

(1) Tsang, W.; Hampson, R. F. *J. Phys. Chem. Ref. Data* **1986**, *15*, 1087.

(2) Warnatz, J. In *Combustion Chemistry*; Gardiner, W. C., Jr., Ed.; Springer-Verlag: New York, 1984.
(3) El Kadi, B.; Baronnet, F. *J. Chim. Phys. PCB* **1995**, *92*, 706.
(4) Bohm, H.; El Kadi, B.; Baronnet, F. *Oxidation Commun.* **1996**, *19*, 25.
(5) Frenklach, M.; Clary, D. W.; Gardiner, W. C.; Stein, S. E. *Symp. Int. Combust. Proc.* **1985**, *20*, 887.
(6) Miller, J. A.; Melius, C. F. *Combust. Flame* **1992**, *91*, 21.
(7) Westmoreland, P. R.; Dean, A. M.; Howard, J. B.; Longwell, J. P. *J. Phys. Chem.* **1989**, *93*, 8171.
(8) Marinov, N. M.; Pitz, W. J.; Westbrook, C. K.; Vincitore, A. M.; Castaldi, M. J.; Senkan, S. M.; Melius, C. F. *Combust. Flame* **1998**, *114*, 192.
(9) Garland, L. J.; Bayes, K. D. *J. Phys. Chem.* **1990**, *94*, 4941.
(10) Fahr, A.; Nayak, A. *Int. J. Chem. Kinet.* **2000**, *32*, 118.
(11) Slagle, I. R.; Gutman, D. *J. Am. Chem. Soc.* **1985**, *107*, 5342.
(12) Stoliarov, S. I.; Knyazev, V. D.; Slagle, I. R. *J. Phys. Chem.* **2000**, *104*, 9687.
(13) Krasnoperov, L. N.; Niiranen, J. T.; Gutman, D.; Melius, C. F.; Allendorf, M. D. *J. Phys. Chem.* **1995**, *99*, 14347.
(14) Daly, N. R. *Rev. Sci. Instrum.* **1960**, *31*, 264.
(15) Lightfoot, P. D.; Kirwan, S. P.; Pilling, M. J. *J. Phys. Chem.* **1988**, *92*, 4938.
(16) Slagle, I. R.; Bernhardt, J. R.; Gutman, D.; Hanning-Lee, M. A.; Pilling, M. J. *J. Phys. Chem.* **1990**, *94*, 3652.
(17) Tulloch, J. M.; Macpherson, M. T.; Morgan, C. A.; Pilling, M. J. *J. Phys. Chem.* **1982**, *86*, 3812.
(18) Slagle, I. R.; Gmurczyk, G. W.; Batt, L.; Gutman, D. *Symp. Int. Combust. Proc.* **1990**, *23*, 115.
(19) Niiranen, J. T.; Gutman, D. *J. Phys. Chem.* **1993**, *97*, 9392−9396.
(20) Bevington, P. R. *Data Reduction and Error Analysis for the Physical Sciences*; McGraw-Hill: New York, 1969.
(21) Slagle, I. R.; Gutman, D.; Davies, J. W.; Pilling, M. J. *J. Phys. Chem.* **1988**, *92*, 2455.
(22) Morter, C. L. F. S. K.; Adamson, J. D.; Glass, G. P.; Curl, R. F. *J. Phys. Chem.* **1994**, *98*, 7029−7035.
(23) Atkinson, D. B.; Hudgens, J. W. *J. Phys. Chem. A.* **1999**, *103*, 4242−4252.
(24) Alkemade, U.; Homann, K. H. *Z. Phys. Chem. (Neue Folge)* **1989**, *161*, 19−34.
(25) Holbrook, K. A.; Pilling, M. J.; Robertson, S. H. *Unimolecular Reactions*, 2nd ed.; Wiley: New York, 1996.
(26) Forst, W. *J. Phys. Chem.* **1972**, *76*, 342.
(27) Pritchard, H. O. *The Quantum Theory of Unimolecular Reactions;* Cambridge University Press: Cambridge, 1984.
(28) Davis, J. W.; Green, N. J. B.; Pilling, M. J. *Chem. Phys. Lett.* **1986**, *129*, 373.
(29) Gilbert, R. G.; Smith, S. C. *Theory of Unimolecular and Recombination Reactions*; Blackwell: Oxford, 1990.
(30) Robinson, P. J.; Holbrook, K. A. *Unimolecular Reactions;* Wiley-Interscience: New York, 1972.
(31) Beyer, T.; Swinehart, D. F. *Commun. ACM* **1973**, *16*, 379.
(32) Astholz, D. C.; Troe, J.; Wieters, W. *J. Chem. Phys* **1979**, *70*, 5107.
(33) Knyazev, V. D. *J. Phys. Chem. A* **1998**, *102*, 3916.
(34) Smith, S. C.; McEwan, M. J.; Gilbert, R. G. *J. Chem. Phys.* **1989**, *90*, 4265.
(35) Mokrushin, V.; Bedanov, V.; Tsang, W.; Zachariah, M. R.; Knyazev, V. D. *ChemRate, Version 1.16*; National Institute of Standards and Technology: Gaithersburg, MD 20899, 1999.
(36) Gaynor, B. J.; Gilbert, R. G.; King, K. D. *Chem. Phys. Lett* **1978**, *55*, 40.
(37) Rabinovitch, B. S.; Tardy, D. C. *J. Chem. Phys.* **1966**, *45*, 3720.
(38) Ellison, G. B.; Davico, G. E.; Bierbaum, V. M.; DePuy, C. H. *Int. J. Mass Spectrom. Ion Processes* **1996**, *156*, 109.
(39) Tsang, W. *Energetics of Organic Free Radicals*; Martinho Simoes, J. A., Greenberg, A., Liebman, J. F., Eds.; Blackie Avademic & Professional: London, 1996.
(40) Pedley, J. B.; Naylor, R. D.; Kirby, S. P. *Thermochemical Data of Organic Compounds*, 2nd ed.; Chapman and Hall: New York, 1986.
(41) Prosen, E. J.; Maron, F. W.; Rossini, F. D. *J. Res. NBS* **1951**, *46*, 106−112.
(42) Liu, X.; Getty, J. D.; Kelly, P. B. *J. Chem. Phys.* **1993**, *99*, 1522.
(43) Botschwina, P.; Oswald, R.; Flugge, J.; Horn, M. *Z. Phys. Chem.* **1995**, *188*, 29−43.
(44) Chase, M. W., Jr. *J. Phys. Chem. Ref. Data* **1998**, *Monogr. 9*, 1.
(45) Durig, J. R.; Compton, D. A. C. *J. Phys. Chem.* **1980**, *84*, 773.
(46) Hirota, E.; Yamada, C.; Okunishi, *J. Chem. Phys.* **1992**, *97*, 2963.
(47) Tanaka, K.; Harada, T.; Sakaguchi, K.; Harada, K.; Tanaka, T. *J. Chem. Phys.* **1995**, *103*, 6450−6458.
(48) Russell, J. J.; Seetula, J. A.; Senkan, S. M.; Gutman, D. *Int. J. Chem. Kinet.* **1988**, *20*, 759.
(49) Dobis, O.; Benson, S. W. *Int. J. Chem. Kinet.* **1987**, *19*, 691.
(50) Bastiansen, O.; Bakken, P.; Kloster-Jensen, E.; Samdal, S.; Traetteberg, M. *J. Mol. Struct.* **1995**, *352/353*, 77−85.
(51) Saussey, J.; Lamotte, J.; Lavalley, J. C. *Spectrochim. Acta, Part A* **1976**, *32*, 763.
(52) Guirgis, G. A.; Durig, J. R.; Bell, S. *J. Mol. Struct.* **1989**, *196*, 101−111.
(53) Kondo, S.; Hirota, E.; Morino, Y. *J. Mol. Spectrosc.* **1968**, *28*, 471.
(54) Murcko, M. A.; Castejon, H.; Wilberg, K. B. *J. Phys. Chem.* **1996**, *100*, 16162.
(55) Knyazev, V. D.; Tsang, W. *J. Phys. Chem. A* **2000**, *104*, 10747.
(56) Feng, Y.; Niiranen, J. T.; Bencsura, A.; Knyazev, V. D.; Gutman, D.; Tsang, W. *J. Phys. Chem.* **1993**, *97*, 871.
(57) Knyazev, V. D. *J. Phys. Chem.* **1995**, *99*, 14738.
(58) Chimbayo, A.; Toselli, B. M.; Barker, J. R. *J. Chem. Phys.* **1998**, *108*, 2383.
(59) Barker, J. R. *Ber. Bunsen-Ges. Phys. Chem.* **1997**, *101*, 566.
(60) Hippler, H.; Troe, J. In *Bimolecular Reactions*; Ashfold, M. N. R., Baggott, J. E., Eds.; The Royal Society of Chemistry: London, 1989.
(61) Oref, I.; Tardy, D. C. *Chem. Rev.* **1990**, *90*, 1407.
(62) Barker, J. R.; Toselli, B. M. *Int. Rev. Phys. Chem.* **1993**, *12*, 305.
(63) Hold, U.; Lenzer, T.; Luther, K.; Reihs, K.; Symonds, A. *Ber. Bunsen-Ges. Phys. Chem.* **1997**, *101*, 552.
(64) Flynn, G. W.; Parmenter, C. S.; Wodtke, A. M. *J. Phys. Chem.* **1996**, *100*, 31.
(65) Tardy, D. C.; Song, B. H. *J. Phys. Chem.* **1993**, *97*, 5628.
(66) Tardy, D. C. *J. Phys. Chem.* **1993**, *97*, 5624.
(67) Kerr, J. A.; Trotman-Dickenson, A. F. *Prog. React. Kinet.* **1961**, *1*, 105.
(68) Blake, A. R.; Henderson, J. F.; Kutschke, K. O. *Can. J. Chem.* **1961**, *39*, 1920.
(69) Robertson, S. H.; Pilling, M. J.; Baulch, D. L.; Green, N. J. B. *J. Phys. Chem.* **1995**, *99*, 13452.
(70) Hessler, J. P.; Ogren, P. J. *J. Phys. Chem.* **1996**, *100*, 984.
(71) Boyd, A. A.; Noziere, B.; Lesclaux, R. *J. Phys. Chem.* **1995**, *99*, 10815.
(72) Jenkin, M. E.; Murrells, T. P.; Shalliker, S. J.; Hayman, G. D. *J. Chem. Soc., Faraday Trans.* **1993**, *89*, 433.